Eigenvalue based taste breaking of staggered, Karsten-Wilczek, and Boriçi-Creutz fermions with stout smearing in the Schwinger model

Maximilian Ammer[1] and Stephan Dürr[1,2]

[1]*Department of Physics, University of Wuppertal, 42119 Wuppertal, Germany*
[2]*Jülich Supercomputing Centre, Forschungszentrum Jülich, 52425 Jülich, Germany*

(Received 12 October 2024; accepted 18 November 2024; published 30 January 2025)

In two spacetime dimensions staggered fermions are minimally doubled, like Karsten-Wilczek and Boriçi-Creutz fermions. A continuum eigenvalue is thus represented by a pair of near-degenerate eigenvalues, with the splitting δ quantifying the cutoff induced taste symmetry breaking. We use the quenched Schwinger model to determine the low-lying fermionic eigenvalues (with 0, 1 or 3 steps of stout smearing) and analyze them in view of the global topological charge $q \in \mathbb{Z}$ of the gauge background. For taste splittings pertinent to would-be zero modes, we find asymptotic Symanzik scaling of the form $\delta_{\mathrm{wzm}} \propto a^2$ with link smearing, and $\delta_{\mathrm{wzm}} \propto a$ without, for each action. For taste splittings pertinent to nontopological modes, staggered splittings scale as $\delta_{\mathrm{ntm}} \propto a^p$ (where $p \simeq 2$ with smearing and $p = 1$ without), while Karsten-Wilczek and Boriçi-Creutz fermions scale as $\delta_{\mathrm{ntm}} \propto a$ (regardless of the smearing level). Large corrections are seen with smearing.

DOI: 10.1103/PhysRevD.111.014511

I. INTRODUCTION

In four spacetime dimensions (4D) staggered fermions offer a discretized version of four Dirac fermions or "tastes" [1]. But they are unequal—two of them have positive and two have negative chirality [2]. Unlike flavor symmetry (which acts on different fields with the same fermion mass) the resulting taste symmetry is not exact, but broken by cutoff effects [3–6]. There is a long stream of efforts which try to mitigate the effect of taste symmetry violation by adding evanescent terms[1] to the staggered action [7–11] and/or by parametrizing the symmetry violation by a dedicated effective field theory description [12,13].

A fresh perspective on the problem was created by the discovery of "minimally doubled" fermions in 4D. Both Karsten-Wilczek (KW) [14,15] and Boriçi-Creutz (BC) [16,17] fermions are in this category. Each one of these formulations encodes two species or tastes (with opposite chiralities), exactly the minimum required by the Nielsen-Ninomiya theorem [2,18,19].

Unfortunately, there is limited knowledge on the actual size of the taste breaking[2] effects of minimally doubled actions and how they fare relative to staggered taste breakings. Staggered fermions are believed to show $O(a^2)$ cutoff effect, due to the (reduced) chiral symmetry [3–6,20]. Both KW and BC fermions have a (reduced) chiral symmetry [14–17], and it has been argued that certain quantities have $O(a^2)$ cutoff effects [21–23]. But it is not clear (to us) whether these arguments cover *all* quantities, in particular the taste splittings.

In two spacetime dimensions (2D) numerical investigations are much cheaper than in 4D. But there is an important difference—in 2D the staggered action is minimally doubled, too. We see this as an opportunity to compare "like with like," that is, three different discretization schemes which encode two species each. Details of minimally doubled fermions in 2D (for instance, with respect to topology and the free-field dispersion relation) have been investigated in Refs. [24–28]. Details of staggered fermions are found in Refs. [3–6,29–32].

We choose the simplest gauge group available, compact $U(1)$. The resulting theory, known as the "Schwinger model" [33,34], resembles QCD in 4D, as it obeys an "index theorem" [35]. This similarity implies that (even close to the continuum) one must be able to sample gauge field configurations with topological

[1]In practice, this is most conveniently done via "smearing" or "gradient flow," see Refs. [7–11].

[2]Throughout, we use "taste breaking" as a shorthand for taste symmetry breaking.

TABLE I. Overview of the ensembles used in the "cutoff effect" study; they implement constant physical volume through $(eL)^2 = (L/a)^2/\beta = 80$. For each choice of $(\beta, L/a)$ three ensembles of 10 000 configurations each are generated, to be used with 0, 1, 3 steps of $\rho = 0.25$ stout smearing, respectively. The analytic result $s^{(0)}_{\text{wils}}$ for unsmeared Wilson glue is taken from Ref. [40], and $p_{\text{inst-hit}}$ denotes the measured acceptance ratio in the instanton hit update routine.

β	3.2	5.0	7.2	12.8	20.0	28.8	51.2	80.0
L/a	16	20	24	32	40	48	64	80
n_{stout}	0, 1, 3	0, 1, 3	0, 1, 3	0, 1, 3	0, 1, 3	0, 1, 3	0, 1, 3	0, 1, 3
$s^{(0)}_{\text{wils}}$	0.17625	0.10662	0.07230	0.03989	0.02533	0.01752	0.00981	0.00627
$p_{\text{inst-hit}}$	0.750(2)	0.737(2)	0.729(2)	0.725(2)	0.726(2)	0.722(2)	0.721(2)	0.721(1)

charge (or "index") $q \in \mathbb{Z}$ ergodically, without "topology freezing." In the Schwinger model this problem has been solved long ago [30,36–39].

The remainder of this article is organized as follows. Section II specifies the update algorithm and how a gauge configuration is assigned a topological charge $q \in \mathbb{Z}$. Section III details how the taste splitting is determined from the low-lying eigenvalues. Section IV investigates how the splittings in a fixed physical volume depend on the lattice spacing a. Section V checks, for fixed a, the volume dependence of these splittings. Section VI presents evidence that the splittings δ obey a Symanzik power law $\delta \propto a^p$ for $a \to 0$. Section VII contains our conclusions, with details of the topological charge determination shifted to the Appendix.

II. SIMULATION SETUP AND TOPOLOGICAL CHARGE DISTRIBUTIONS

We simulate the quenched Schwinger model with the Wilson gauge action

$$S[U] = \beta \sum_x \{1 - \text{Re}[U_\square(x)]\} \quad \text{with}$$
$$U_\square(x) = U_1(x) U_2(x+\hat{1}) U_1^*(x+\hat{2}) U_2^*(x) \tag{1}$$

where $\hat{\mu}$ denotes a times the unit vector in direction μ, and U^* is the complex conjugate of the unit-modulus variable U. Alternatively, one might parametrize it as $U_\mu(x) = e^{i\varphi_\mu(x)}$ with $\varphi \in]-\pi, \pi]$, and substitute $\text{Re}[.] \to \cos[\varphi_1(x) + \varphi_2(x+\hat{1}) - \varphi_1(x+\hat{2}) - \varphi_2(x)]$ in (1).

We use multihit-Metropolis and overrelaxation sweeps in a $1 \div 4$ ratio and augment these packages with instanton hits (proposing a $q \to q \pm 1$ update, which is accepted with a probability that tends to 1 in the infinite volume limit, see Tables I and II) and parity hits (proposing a $q \to -q$ update which is always accepted). With these ingredients it is easy to generate well decorrelated configurations (see Ref. [38] for details).

After the configurations are generated, we smear them with n stout steps at $\rho = 0.25$ [41], and on the smeared backgrounds we evaluate the two topological charges [6,30]

$$q^{(n)}_{\text{geo}} \equiv \frac{1}{2\pi} \sum_x \text{Im} \log U^{(n)}_\square(x) = \frac{1}{2\pi} \sum_x [\varphi^{(n)}_1(x) + \varphi^{(n)}_2(x+\hat{1}) - \varphi^{(n)}_1(x+\hat{2}) - \varphi^{(n)}_2(x)]_{]-\pi,\pi]} \tag{2}$$

$$q^{(n)}_{\text{raw}} \equiv \frac{1}{2\pi} \sum_x \text{Im}\, U^{(n)}_\square(x) = \frac{1}{2\pi} \sum_x \sin[\varphi^{(n)}_1(x) + \varphi^{(n)}_2(x+\hat{1}) - \varphi^{(n)}_1(x+\hat{2}) - \varphi^{(n)}_2(x)] \tag{3}$$

where $U^{(n)}_\square(x)$ is the 4-link product in (1) after $n \in \{0, 1, 3\}$ smearing steps. The "geometric charge" (2) is integer valued, while (3) is not. But the distribution of the latter is strongly peaked at near-integer values $\mathbb{Z}/Z$ with $Z > 1$. Hence, one defines the "field-theoretic charge"

TABLE II. Overview of the ensembles used in the "finite volume" study; each one contains 10 000 configurations and is used after a single step of $\rho = 0.25$ stout smearing. In addition, the acceptance rate of the instanton hit update (see text) at the respective $(\beta, L/a)$ is given.

β	7.2	7.2	7.2	7.2	7.2	7.2
L/a	16	20	24	32	40	48
n_{stout}	1	1	1	1	1	1
$p_{\text{inst-hit}}$	0.597(2)	0.677(2)	0.729(2)	0.799(2)	0.838(2)	0.866(2)

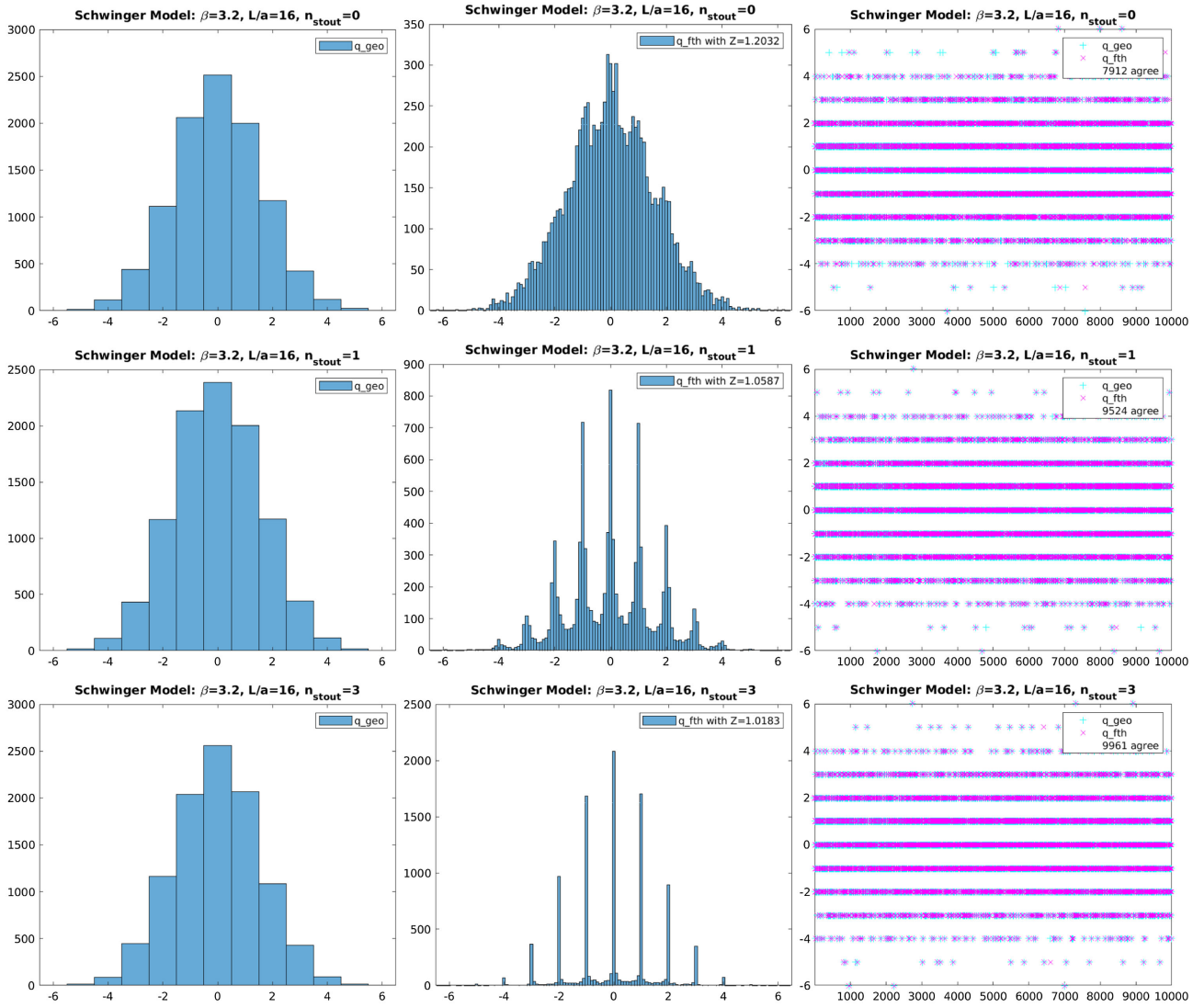

FIG. 1. Histograms (for our coarsest ensembles) of the integer-valued topological charge q_{geo} (left) and of the real-valued Zq_{raw} (middle), along with the resulting MC time histories of q_{geo} and q_{fth} after rounding (right) with 0 (top), 1 (middle) and 3 (bottom) stout smearings. The three rows refer to three different ensembles of 10 000 configurations each at $(\beta, L/a) = (3.2, 16)$.

$$q_{\mathrm{fth}}^{(n)} = \mathrm{round}(Zq_{\mathrm{raw}}^{(n)}) \tag{4}$$

which is again integer valued. We determine $Z = Z(\beta, n)$ nonperturbatively, with details given in the Appendix. In a particular run only one smearing level is realized, and the resulting configuration $U^{(n)}$ is assigned a topological charge $q^{(n)}$ if and only if $q_{\mathrm{geo}}^{(n)} = q_{\mathrm{fth}}^{(n)}$ holds true.[3] Figure 1 presents the histograms of $q_{\mathrm{geo}}^{(n)}$ and $q_{\mathrm{fth}}^{(n)}$ at our coarsest lattice spacing ($\beta = 3.2$) for the stouting levels $n \in \{0, 1, 3\}$. The respective Monte Carlo (MC) time histories look ergodic and the fraction of configurations without charge assignment diminishes quickly with increasing n and/or increasing β.

In a given run the smearing level $n \in \{0, 1, 3\}$ is kept fixed, and the matrices D_{st}, D_{KW} and D_{BC} are evaluated on the respective background $U^{(n)}$. These operators refer to the Susskind "staggered" [1], Karsten-Wilczek [14,15] and Boriçi-Creutz [16,17] definitions of the massless Dirac matrix, respectively. For each formulation the 16 smallest eigenvalues $\mathrm{i}\lambda$ on the positive[4] imaginary axis are determined and the $\lambda > 0$ are archived. This way the eigenvalues of different formulations are statistically correlated, but the different smearing levels are not.

[3] In principle also the integer-valued staggered topological charge $q_{\mathrm{stag}}^{(n)}$ might be evaluated, see e.g. Ref. [28] for details in 2D and a guide to the literature. Due to the increased CPU demand, we refrain from doing so.

[4] The eigenvalues come in $\pm\mathrm{i}\lambda$ pairs, due to ϵ-hermiticity or γ_5-hermiticity, respectively.

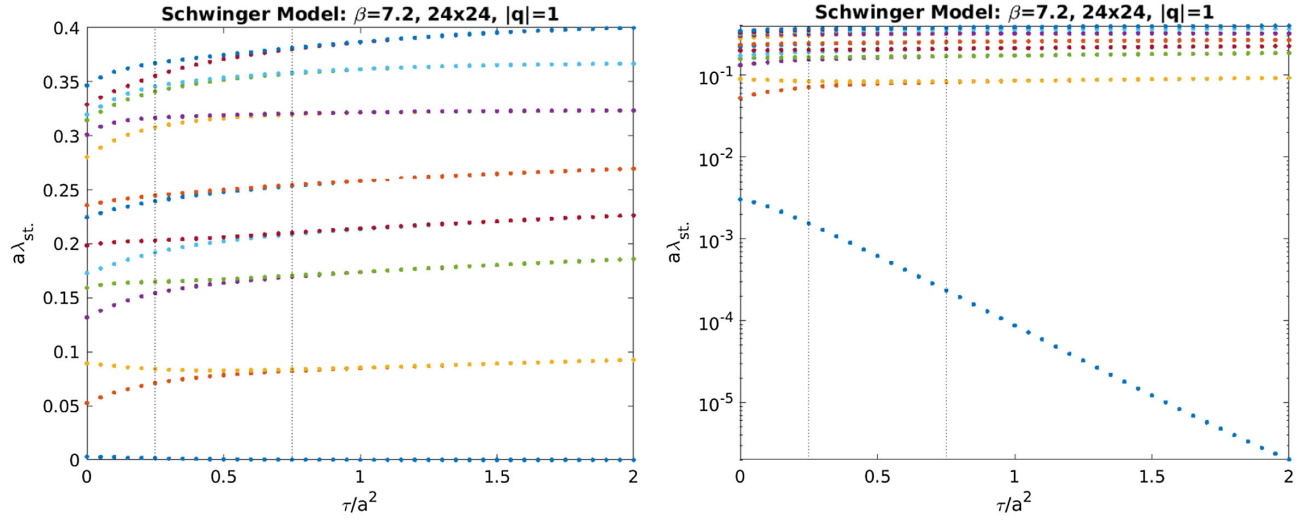

FIG. 2. Eigenvalues $a\lambda_j$ $(1 \le j \le 15)$ of $D_{\mathrm{st}}/\mathrm{i}$ on a $|q| = 1$ configuration at $(\beta, L/a) = (7.2, 24)$ versus the gradient flow time τ/a^2, in standard (left) and logarithmic (right) representation.

The Schwinger model (with any N_f) is superrenormalizable, and the gauge coupling e has mass-dimension one. We exploit this feature to set the lattice spacing via $ae = 1/\sqrt{\beta}$. This way it is easy to define simulation parameters which implement a continuum limit "at constant physics" (i.e. fixed box size and possibly pion mass in physical units), see Table I. We produce an additional set of ensembles to investigate finite volume effects, see Table II and pertinent comments in Sec. V. In total this gives $3 \times 8 + 5 = 29$ ensembles for which we checked that the unsmeared plaquette agrees, within errors, with the analytic result of Ref. [40].

III. ANALYSIS DETAILS ON CENTRAL ENSEMBLE

The gauge ensemble with $(\beta, L/a, n_{\mathrm{stout}}) = (7.2, 24, 1)$ appears both in Tables I and II. We call it the "central ensemble" and use it to specify the details of our analysis.

In 2D the (rotated) eigenvalues $0 < \lambda_1 < \ldots < \lambda_{16}$ of an operator D_{st}, D_{KW} or D_{BC} come in near-degenerate pairs (in 4D the staggered ones come in quartets [42,43]). However, the details of the grouping depend on the absolute value of the topological charge of the background. For $q = 0$ the pairing is $\lambda_1 \simeq \lambda_2, \lambda_3 \simeq \lambda_4, \ldots, \lambda_{15} \simeq \lambda_{16}$, based on the fact that the intrataste splitting is smaller than the physical eigenvalue splitting. In this case $\sum_{j=1}^{8} \lambda_{2j} - \lambda_{2j-1}$ would be a suitable measure of the taste breaking effect on this background. For $|q| = 1$ things are different, since λ_1 is the archived part of the would-be zero mode pair $\pm\lambda_1$. In this case $2\lambda_1 + \sum_{j=1}^{7} \lambda_{2j+1} - \lambda_{2j}$ is an appropriate measure of the taste breaking effect (where we made sure that again eight splittings are taken into account). Similarly, for $|q| = 2$, one needs to keep in mind that $-\lambda_1, \lambda_1$ is one pair and $-\lambda_2, \lambda_2$ another one. Hence, in this case we prefer to use $2\lambda_1 + 2\lambda_2 + \sum_{j=1}^{6} \lambda_{2j+2} - \lambda_{2j+1}$, and so on.

One may also consider each splitting separately, for instance $\{2\lambda_1, 2\lambda_2, \lambda_4 - \lambda_3, \ldots, \lambda_{14} - \lambda_{13}\}$ in the $|q| = 2$ case, and this is what we shall do in the following. Throughout, the operator D_{st}, D_{KW} or D_{BC} and the charge q involve the same amount of link smearing, i.e. $n \in \{0, 1, 3\}$ steps of stout smearing [41] in both cases.

Figure 2 displays, for a configuration with $|q| = 1$, how the staggered eigenvalues $a\lambda_j$ evolve as a function of the gradient flow time τ/a^2 [44]. The would-be zero mode $a\lambda_1$ (to be paired with its negative) goes to zero, all other modes form pairs that become gradually visible as the flow time increases. Both the would-be zero mode and the remaining splittings (e.g. $a\delta_2 = a\lambda_3 - a\lambda_2$) decrease *exponentially* in the gradient flow time, see Fig. 3 and

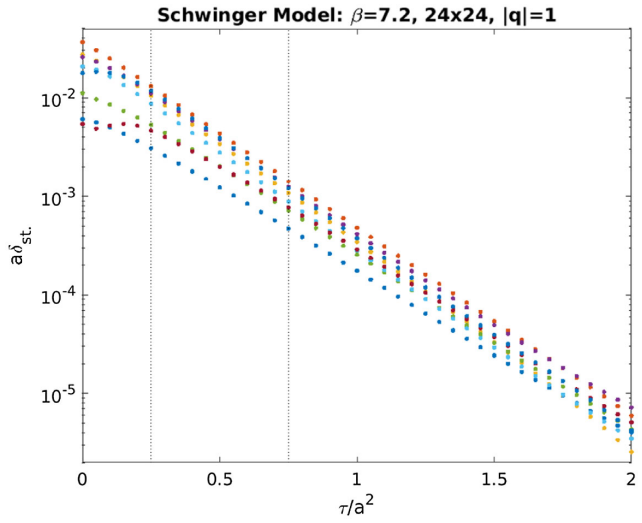

FIG. 3. Staggered taste splittings $a\delta_1 \equiv 2a\lambda_1, a\delta_2 \equiv a\lambda_3 - a\lambda_2, \ldots, a\delta_8 \equiv a\lambda_{15} - a\lambda_{14}$ (as appropriate for $|q| = 1$) in logarithmic representation, derived from the data shown in Fig. 2.

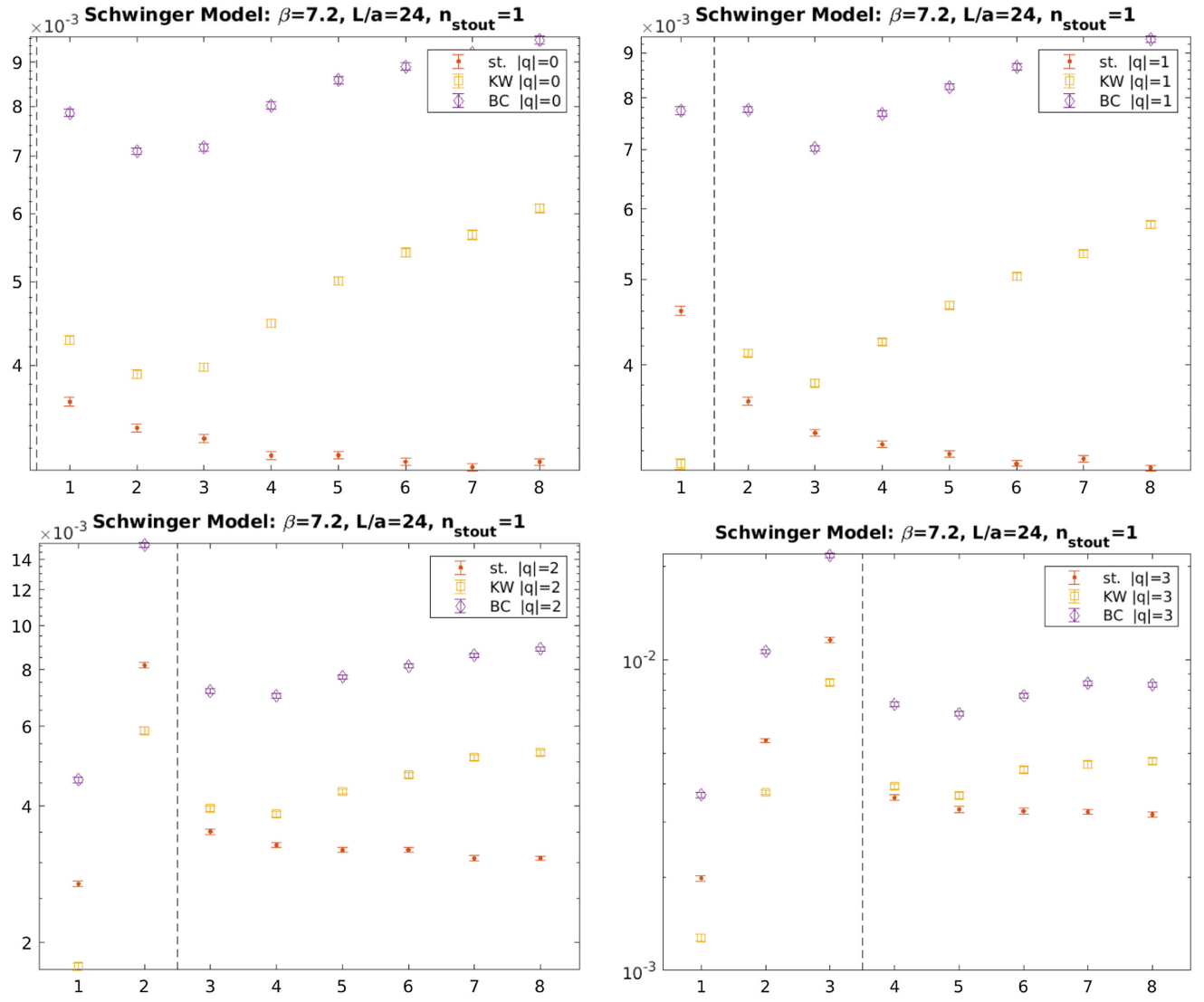

FIG. 4. Taste splittings $a\delta_j$ $(1 \le j \le 8)$ of the operators D_{st}, D_{KW} and D_{BC} on the central ensemble. The would-be zero mode splittings $a\delta_1, \ldots, a\delta_{|q|}$ are separated from the nontopological splittings $a\delta_{|q|+1}, \ldots$ by a dashed vertical line. The four panels refer to $|q| = 0$, 1, 2, 3, respectively. Both the operator and the charge measurement involve one step of stout smearing.

Ref. [45]. The flow times $\tau/a^2 = 0.25$, 0.75 used in the main investigation (modulo discretization effects in τ [44]) are marked with dotted vertical lines. Hence, with one step of $\rho = 0.25$ stout smearing at $\beta = 7.2$ the eigenvalue pairs are faintly visible, and with three steps they are easily identified.

Figure 4 displays the taste splittings $a\delta_j$ on our central ensemble $(\beta, L/a, n_{\mathrm{stout}}) = (7.2, 24, 1)$ in which all 10 000 configurations are assigned[5] a topological charge. The first panel shows the results on the 2697 configurations with $q = 0$; here staggered fermions feature the smallest taste breakings. The second and third panels show the situation on the 4320 and 2147 configurations with $|q| = 1$ and $|q| = 2$, respectively. The fourth panel repeats this for the 661 configurations with $|q| = 3$. Throughout, the would-be zero mode splittings are separated by a vertical dashed line, and those of KW fermions seem particularly small. The topological sectors $4 \le |q| \le 6$ hold too few $(151 + 20 + 4)$ configurations for a statistical analysis.

In short, on the central ensemble no dramatic differences between the three fermion operators are observed. For nontopological modes the staggered action shows the smallest taste splittings, but for splittings linked to would-be zero modes the KW action performs better. Hence, the question is whether this remains true as we vary the smearing level and/or the lattice spacing (Sec. IV). Also the impact of the box volume deserves a closer look (Sec. V).

[5]Respective numbers are 9524 for $\beta = 3.2$, 9989 for $\beta = 5.0$ and 10 000 for $\beta \ge 7.2$ at $n_{\mathrm{stout}} = 1$, cf. Table I.

IV. LATTICE SPACING DEPENDENCE

As mentioned in Sec. II, we have the data to investigate how the unwanted taste splitting changes if the lattice spacing is varied at fixed (physical) box volume.

Let us recap the second panel ($|q| = 1$) of Fig. 4, which was for $(\beta, L/a, n_{\text{stout}}) = (7.2, 24, 1)$. For the nontopological splittings ($j \geq 2$) there is a hierarchy $\delta_{\text{st}} < \delta_{\text{KW}} < \delta_{\text{BC}}$. For the would-be zero mode splitting ($j = 1$), there is an inversion, since we find $\delta_{\text{KW}} < \delta_{\text{st}} < \delta_{\text{BC}}$.

The counterparts to this panel at coarser and finer lattice spacings are shown in Fig. 5, still with $n_{\text{stout}} = 1$. The most prominent change is a change in the y-axis label. At $\beta \in \{3.2, 5.0\}$ the situation resembles the one of the central ensemble, except that δ_j^{KW} wins for a few more j. At weaker coupling, i.e. for $\beta \in \{12.8, 20.0\}$, the staggered splittings get progressively smaller (starting with the higher j) than the splittings of KW or BC fermions. However, the would-be zero mode (to the left of the dashed vertical line) seems to be exempt from this rule; here the KW splitting remains smaller than any other splitting. We have three finer lattice spacings ($\beta = 28.8$, 51.2, 80.0), but the situation remains similar to the one shown in the fourth panel. Hence, close enough to the continuum, there is a difference between would-be zero modes and nontopological modes. For large enough β the staggered action wins the contest for nontopological modes. By contrast, for the first would-be zero mode the KW fermion features the smallest splitting at all accessible lattice spacings.

On may ask whether it makes a difference if we choose fewer ($n_{\text{stout}} = 0$) or more ($n_{\text{stout}} = 3$) smearing steps. Figure 6 presents these alternatives to the third panel

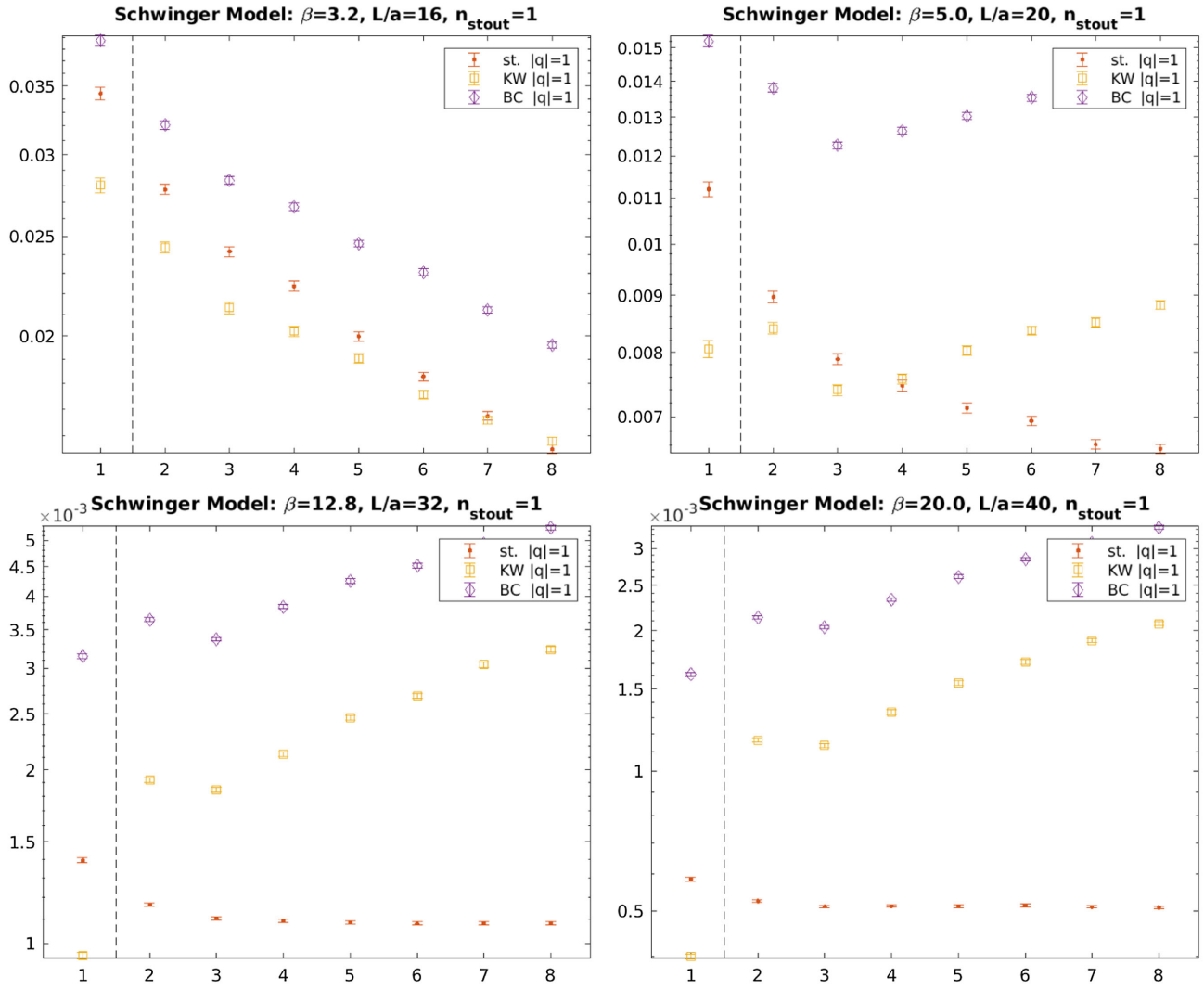

FIG. 5. Counterparts to the second ($|q| = 1$) panel of Fig. 4, with coarser ($\beta = 3.2$, 5.0) and finer ($\beta = 12.8$, 20.0) lattice spacings, respectively. The smearing level is $n_{\text{stout}} = 1$ throughout.

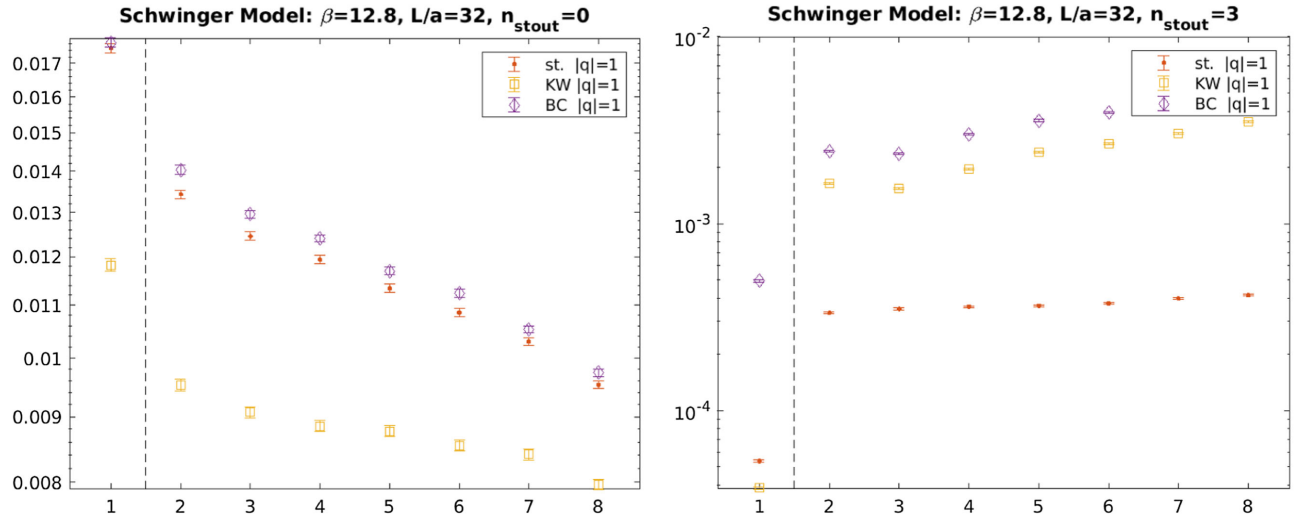

FIG. 6. Counterparts to the third ($\beta = 12.8$) panel of Fig. 5, with $n_{\text{stout}} = 0$, 3, respectively.

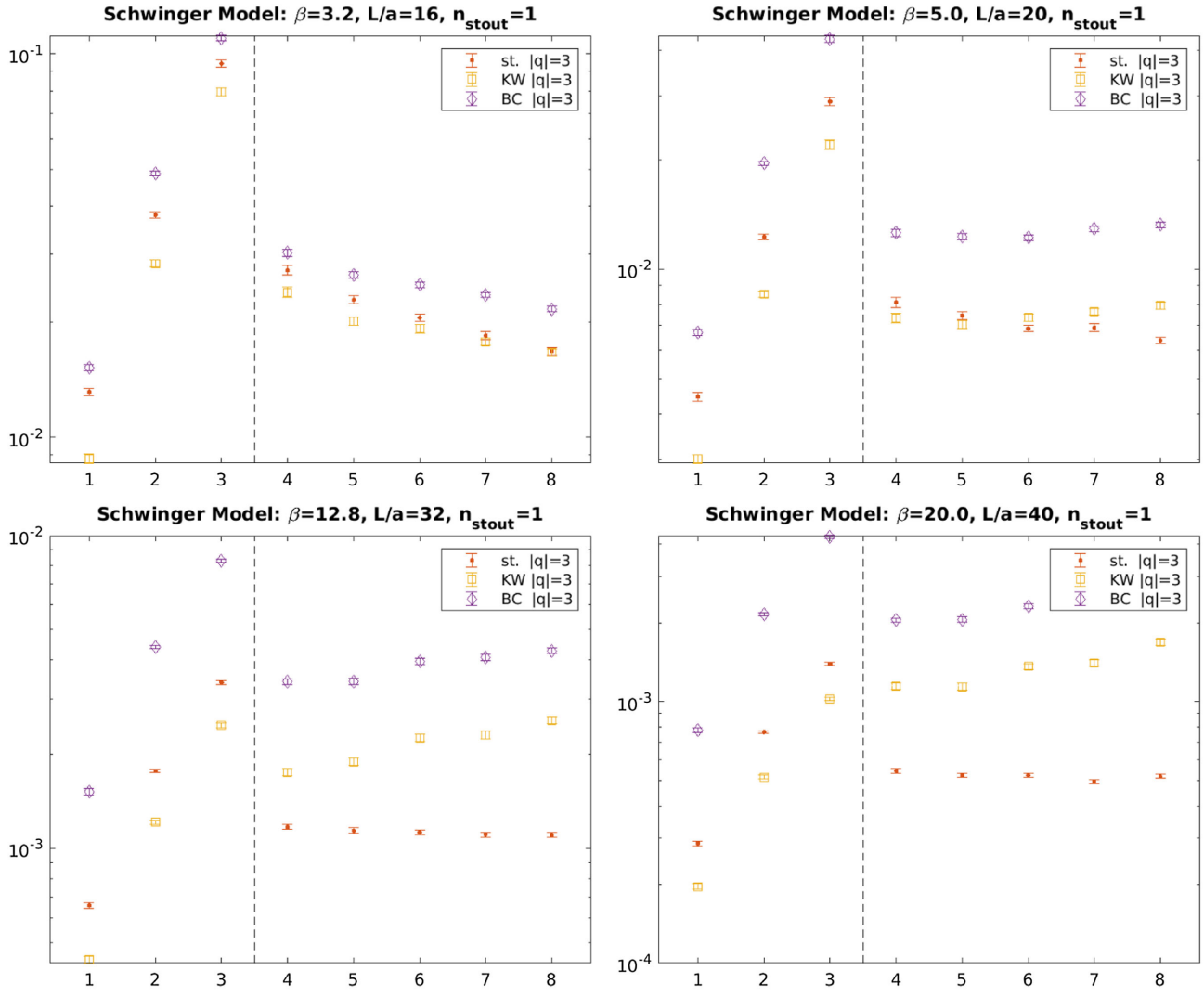

FIG. 7. Counterparts to the fourth ($|q| = 3$) panel of Fig. 4, with coarser ($\beta = 3.2$, 5.0) and finer ($\beta = 12.8$, 20.0) lattice spacings, respectively. The smearing level is $n_{\text{stout}} = 1$ throughout.

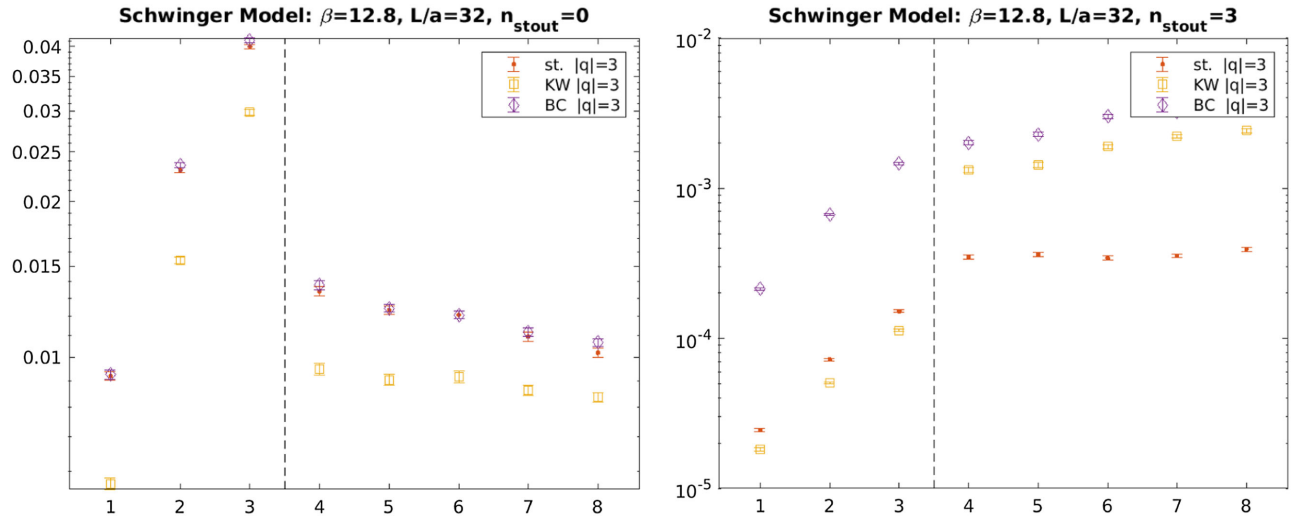

FIG. 8. Counterparts to the third ($\beta = 12.8$) panel of Fig. 7, with $n_{\text{stout}} = 0$, 3, respectively.

($\beta = 12.8$) of Fig. 5. In fact, the $n_{\text{stout}} = 0$ panel resembles the first panel in the previous figure, and the $n_{\text{stout}} = 3$ panel is similar to the fourth panel in the previous figure. It seems that increasing/decreasing the smearing level acts a bit like[6] increasing/decreasing β.

In Fig. 7 the eigenvalue splittings of the $|q| = 3$ configurations at $\beta = 3.2$, 5.0, 12.8, 20.0 with $n_{\text{stout}} = 1$ are shown. Together with the fourth panel of Fig. 4 they constitute a "line of constant physics". The qualitative difference between nontopological modes ($j = 1$, 2, 3) and would-be zero modes ($j \geq 4$) is quite obvious. The three lattice spacings not shown ($\beta = 28.8$, 51.2, 80.0) feature a situation similar to one shown in the last panel. Hence, for the nontopological modes the staggered action wins the contest at large enough β, followed by KW and BC fermions. For the would-be zero modes, on the other hand, the KW splitting is always smaller than the staggered one, and the latter fares better than the BC splitting.

In Fig. 8 the third panel ($\beta = 12.8$) of Fig. 7 is confronted with its siblings at $n_{\text{stout}} = 0$ and $n_{\text{stout}} = 3$. Again the left panel resembles the first panel of the previous figure, and the right panel resembles the fourth panel of the previous figure. Overall it seems that an increased smearing level gives a "preview" of a larger β (with the caveat mentioned above).

In short, varying the cutoff (at fixed $n_{\text{stout}} = 1$) confirms the different behavior of would-be zero modes and nontopological modes. For the latter category the staggered action yields asymptotically smaller splittings than either minimally doubled action. On the other hand, for the former category the KW action features the smallest splittings at all $(\beta, n_{\text{stout}})$ combinations explored. We shall speculate on possible reasons for this observation in Sec. VI.

V. FINITE VOLUME EFFECTS

As mentioned in Sec. II, we have the data needed to investigate how the unwanted taste splitting changes if the (physical) box volume is varied at fixed lattice spacing.

The data in Fig. 9 extend the third panel ($|q| = 2$) of Fig. 4 toward smaller and larger box sizes, keeping $(\beta, n_{\text{stout}}) = (7.2, 1)$ fixed. Evidently, the box volume impacts the overall scale, but it does not affect the hierarchy among the eigenvalue splittings. In particular the distinction between would-be zero modes and nontopological modes holds in the sense that for these parameters the hierarchies $\delta_{\text{KW}} < \delta_{\text{st}} < \delta_{\text{BC}}$ for would-be zero modes and $\delta_{\text{st}} < \delta_{\text{KW}} < \delta_{\text{BC}}$ for nontopological modes hold in all volumes.

We conclude that the data presented in Sec. IV have been collected in a large enough physical volume to avoid relevant finite volume effects on the splittings. Hence the question whether we understand the observed lattice spacing dependence is well warranted. As an aside we find that the *instanton hit acceptance ratio* depends in the first place on the *physical volume*; the data in Fig. 10 (right)

[6]Of course, this statement is to be taken with a grain of salt; one should stay away from "oversmearing," as this will cause a lot of near degeneracies among the eigenvalues, similar to the free-field case where excessive degeneracies emerge. We maintain that all our smearing levels, $n_{\text{stout}} = 0$, 1, 3, represent *mild* smearings, since the integrated flow times $\tau/a^2 = 0.0$, 0.25, 0.75 yield diffusion lengths in lattice units $\sqrt{4\tau}/a \simeq 0.0$, 1.0, 1.73, respectively [44]. We expect that the effects of oversmearing would show up in the regime $\tau/a^2 \gg 1$.

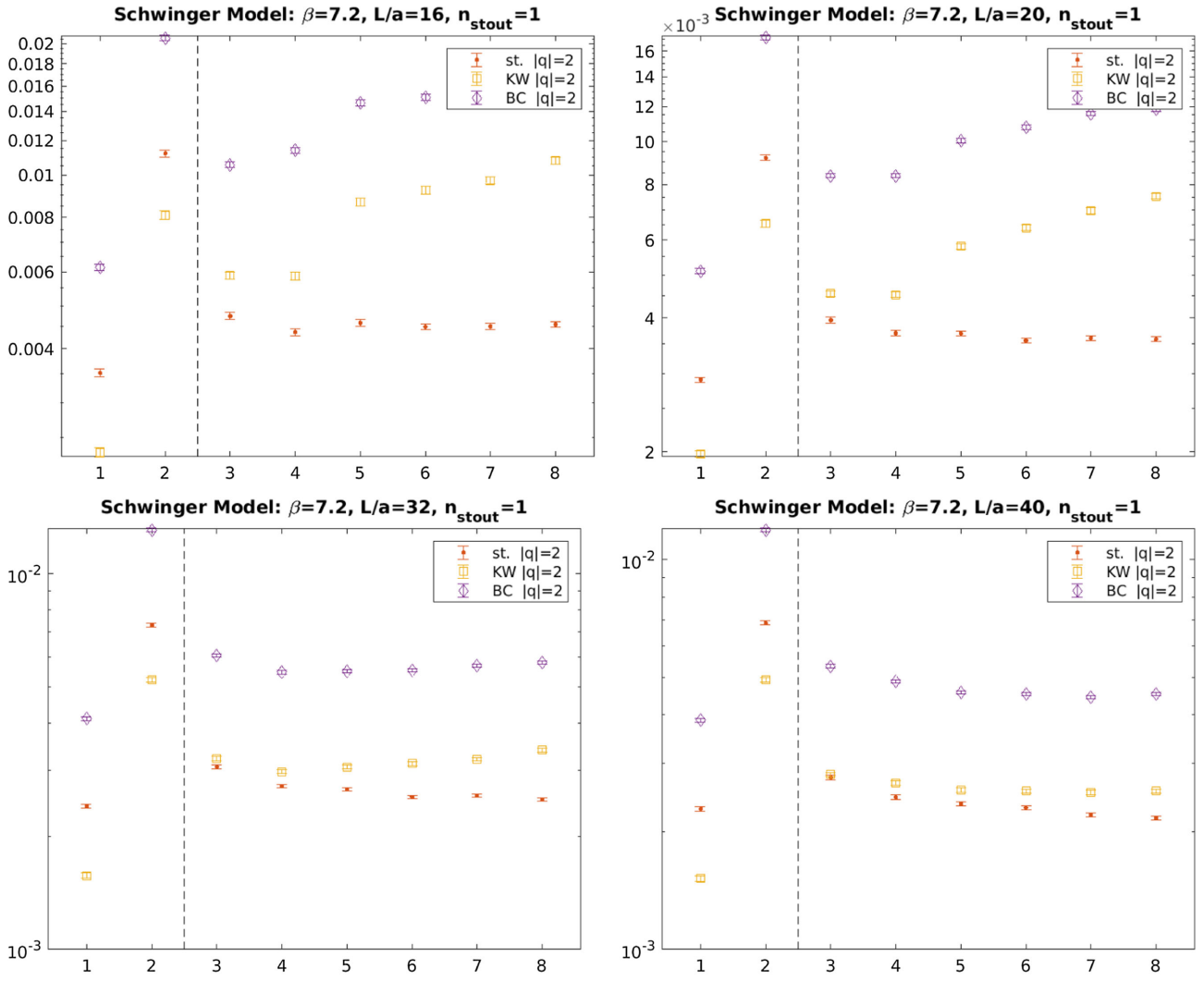

FIG. 9. Counterparts to the third ($|q| = 2$) panel of Fig. 4, with smaller ($L/a = 16$, 20) and larger ($L/a = 32$, 40) box size, respectively. Throughout $(\beta, n_{\text{stout}}) = (7.2, 1)$ is kept fixed.

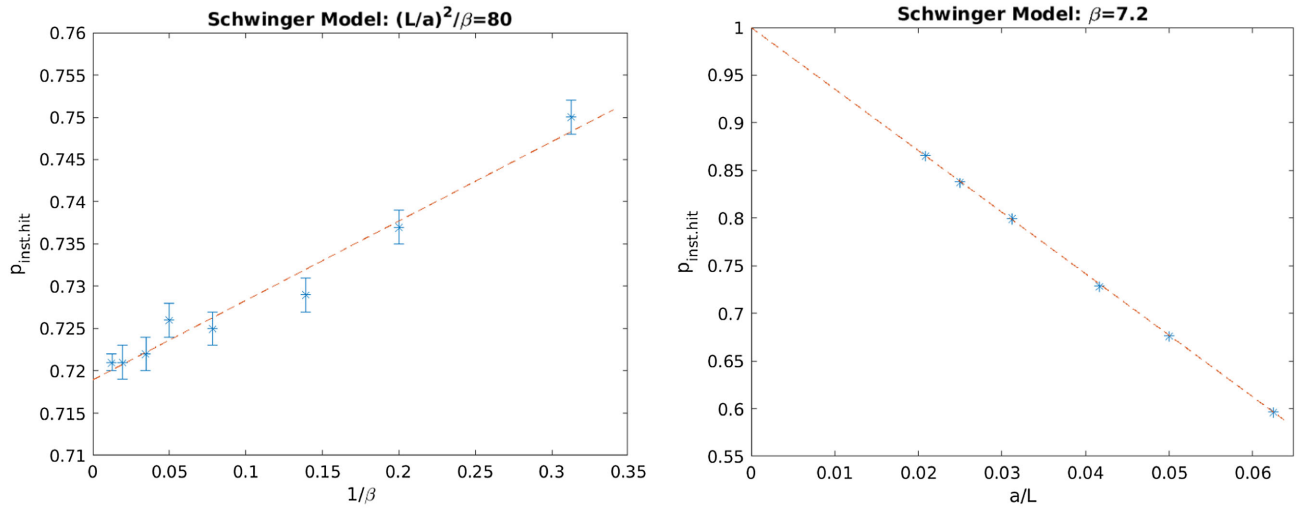

FIG. 10. Instanton hit acceptance ratio $p_{\text{inst-hit}}$ versus $1/\beta$ in a fixed physical volume (left and Table I) and versus a/L at fixed β (right and Table II), along with linear fits.

suggest that $p_{\text{inst-hit}} \to 1$ holds in the limit $L \to \infty$ for any β.

VI. SYMANZIK SCALING OF TASTE SPLITTINGS

So far we found that it makes a difference whether a given eigenvalue belongs to a would-be zero mode or a nontopological mode. For would-be zero modes KW fermions win[7] the contest; their splittings are smaller than those of staggered or BC fermions at any $(\beta, n_{\text{stout}})$ explored. For nontopological modes staggered fermions yield the smallest intrataste splittings if $n_{\text{stout}} \geq 1$. These findings are presented in Figs. 4–9.

The next step is to check whether a given splitting shows asymptotic Symanzik scaling and, if so, to determine its universality class (i.e. the power p in $\delta \propto a^p$) [46–49]. For this purpose one needs to collect all data pertinent to a given Dirac operator, smearing level and splitting type (i.e. treating would-be zero modes and nontopological modes separately), and investigate their dependence on the lattice spacing $a \propto \beta^{-1/2}$. For staggered fermions standard reasoning suggests that the taste splittings in physical units (with mass-dimension one) scale as $\delta_i \propto a^2$ (tantamount to $a\delta_j \propto a^3$ in lattice units) for all j, unless the measurement operator reduces the power. For KW and BC fermions things are more involved, since their chiral symmetry groups[8] are smaller. Still, there are results in the literature which suggest leading $O(a^2)$ cutoff effects for these fermion formulations [21–23], but in some cases[9] results are inconclusive.

We shall first address the would-be zero mode splittings, followed by those of the nontopological modes. Figure 11 displays the would-be zero mode splittings of each fermion formulation at $n_{\text{stout}} = 0$ as a function of a in log-log representation. For $|q| = 1$ there is one splitting (top left panel), for $|q| = 2$ there are two splittings (top right and middle left), and for $|q| = 3$ there are three such splittings (remaining three panels). Without smearing all formulations seem to have asymptotic behavior $a\delta_j \propto a^2$ or $\delta_i \propto a$ for this observable. This is perhaps acceptable for KW and BC fermions, but it is *worse* than expected for staggered fermions.

In Fig. 12 the would-be zero mode splittings of each formulation at $n_{\text{stout}} = 1$ are plotted as a function of a in log-log representation. This time the data suggest an asymptotic scaling behavior $\delta_i \propto a^2$ for *all three* formulations. There are substantial corrections to the asymptotic behavior, even though we simulate rather fine[10] Schwinger model lattices.

In Fig. 13 the taste violations pertinent to would-be zero modes at $n_{\text{stout}} = 3$ are plotted as a function of a in log-log representation. Like in the previous figure, the would-be zero mode splittings scale as $\delta_i \propto a^2$ for all three fermion operators, but with the additional smearing steps the subleading corrections seem even more pronounced.

Note that the dotted lines in these figures are no fits. They show the Symanzik behavior $\delta \propto a^p$ with the conjectured power p, starting from the leftmost data point. This way one can gauge the size of corrections by visual inspection.

We now turn to the nontopological modes. Figure 14 displays these splittings for each fermion formulation at $n_{\text{stout}} = 0$ as a function of a in log-log representation. For $q = 0$ it is $a\delta_1 = a\lambda_2 - a\lambda_1$ (top left panel), for $|q| = 1$ it is $a\delta_2 = a\lambda_3 - a\lambda_2$ (top right panel), and analogously for $|q| = 2$ (lower left panel) and $|q| = 3$ (lower right panel). Without smearing all formulations seem to have asymptotic behavior $a\delta_j \propto a^2$ or $\delta_i \propto a$ for this observable. Again, this seems acceptable for KW and BC fermions, but it is worse than expected for staggered fermions.

In Fig. 15 results for taste violations pertinent to nontopological modes at $n_{\text{stout}} = 1$ are plotted as a function of a in log-log representation. Here the asymptotic behavior depends on the Dirac operator; we find $\delta_i \propto a^2$ for D_{st} and $\delta_i \propto a$ for D_{KW}, D_{BC}. The data suggest that there are substantial corrections to the asymptotic behavior for $\beta < 20$.

In Fig. 16 the same information is shown with $n_{\text{stout}} = 3$ smearings. Results are similar to those in the previous figure, except that the sign of the corrections seems reversed, and the staggered nontopological splittings require truly large β-values, at this level of smearing, to show asymptotic Symanzik scaling.

Clearly, the most puzzling observation is that the Symanzik power of staggered taste breakings seems to depend on the smearing level. Without smearing we see $\delta_j^{\text{st}} \propto a$, with smearing we find $\delta_j^{\text{st}} \propto a^2$. For any fixed (ρ, n_{stout}) combination the smearing amounts to an *ultralocal modification* of D_{st}; the asymptotic behavior should be insensitive to such a modification. Of course, it is conceivable that any of our Figs. 11–16 do not reflect the true asymptotic behavior, but in view of the large β-values this would be surprising. For further discussion we summarize the conjectured powers p, as suggested by our data, in Table III.

[7]This solidifies and extends an observation reported in Ref. [28].

[8]See Ref. [50] for a thorough analysis of the symmetry groups of KW and BC fermions.

[9]For instance Ref. [27] finds that the real part of the BC dispersion relation has leading cutoff effects $O([am]^2)$, while the imaginary part has $O(am)$ cutoff effects.

[10]At two β-values the unsmeared plaquette $1 - s_{\text{wil}}^{(0)}$ is above 0.99 and at three more above 0.96, see Table I.

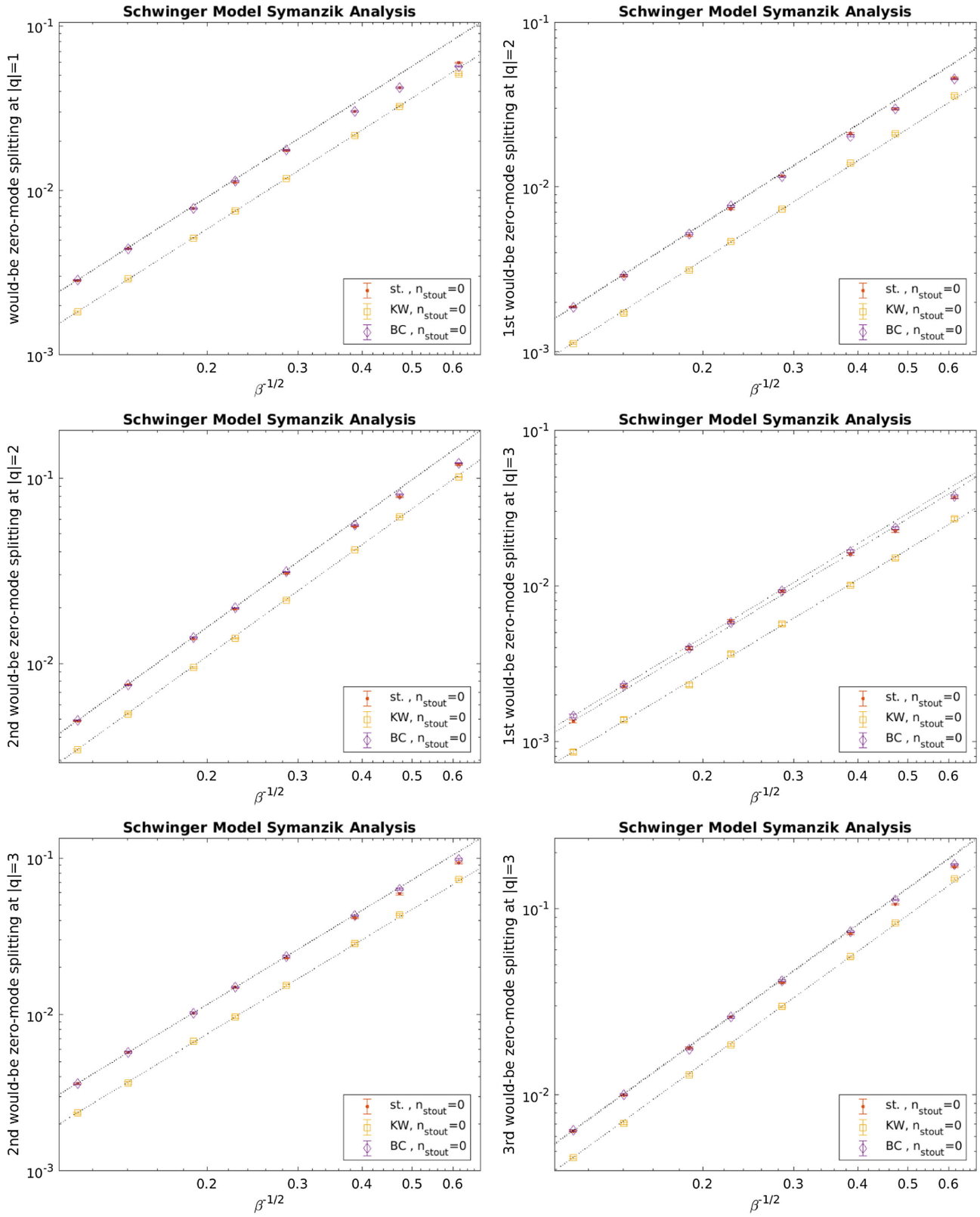

FIG. 11. All would-be zero mode splittings $a\delta_j$ at $|q| = 1, 2, 3$ versus a for $n_{\text{stout}} = 0$. For each operator the dotted line is a power law $a\delta \propto a^2$, going through the leftmost data point.

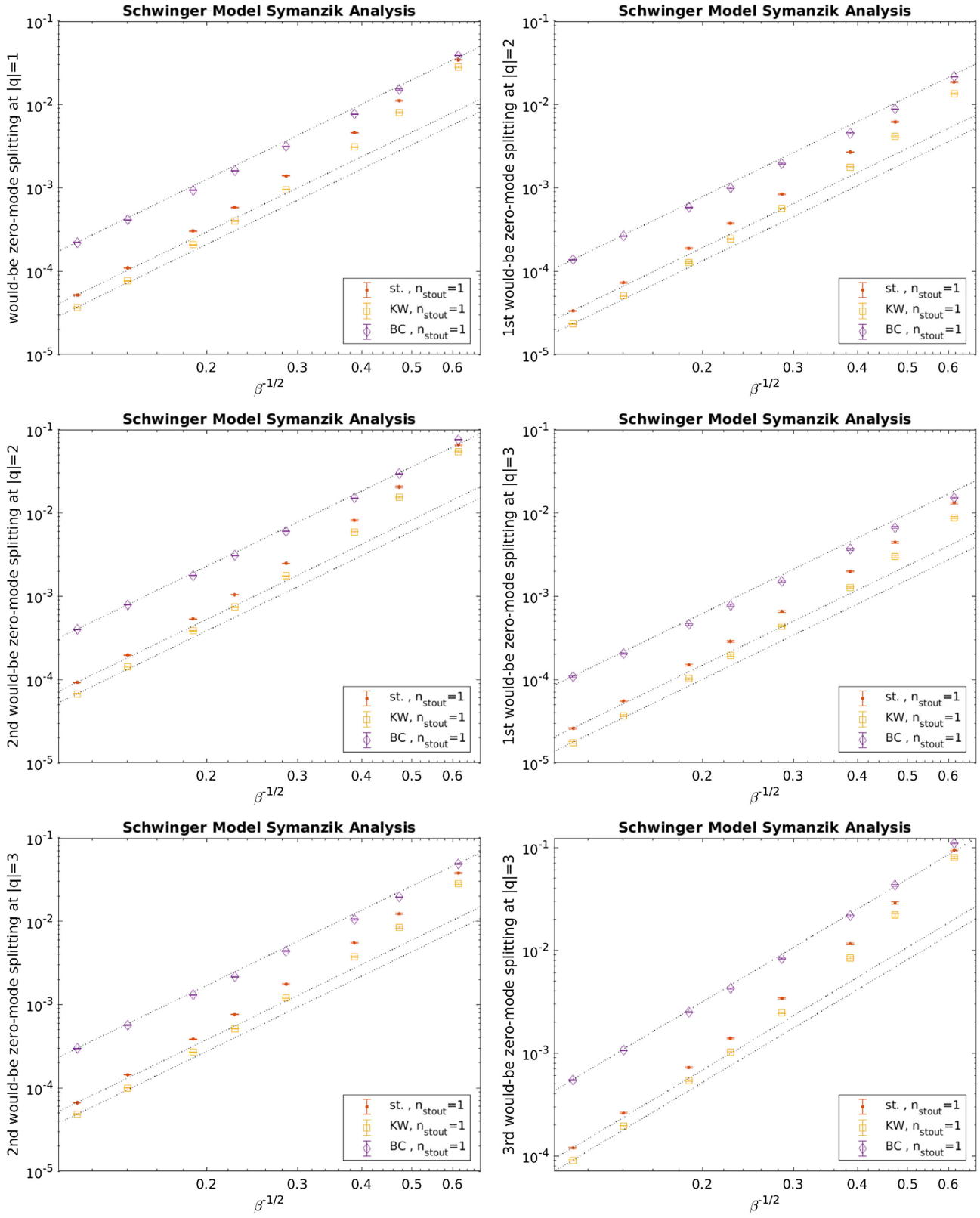

FIG. 12. Same as Fig. 11 but for $n_{\mathrm{stout}} = 1$. For each operator the dotted line is a power law $a\delta \propto a^3$ (i.e. a higher power than in Fig. 11), going through the leftmost data point.

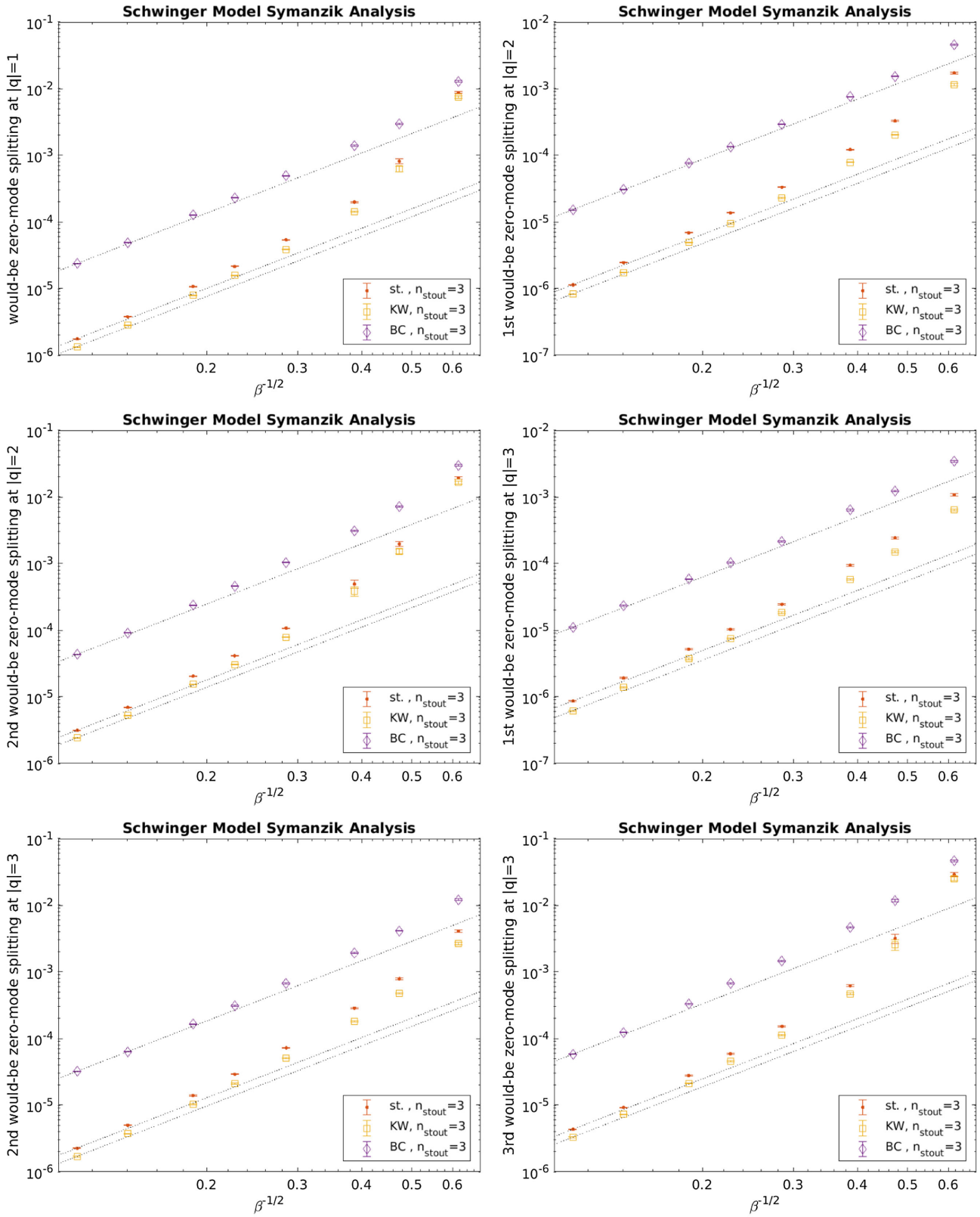

FIG. 13. Same as Fig. 11 but for $n_{\mathrm{stout}} = 3$. For each operator the dotted line is a power law $a\delta \propto a^3$ (i.e. a higher power than in Fig. 11), going through the leftmost data point.

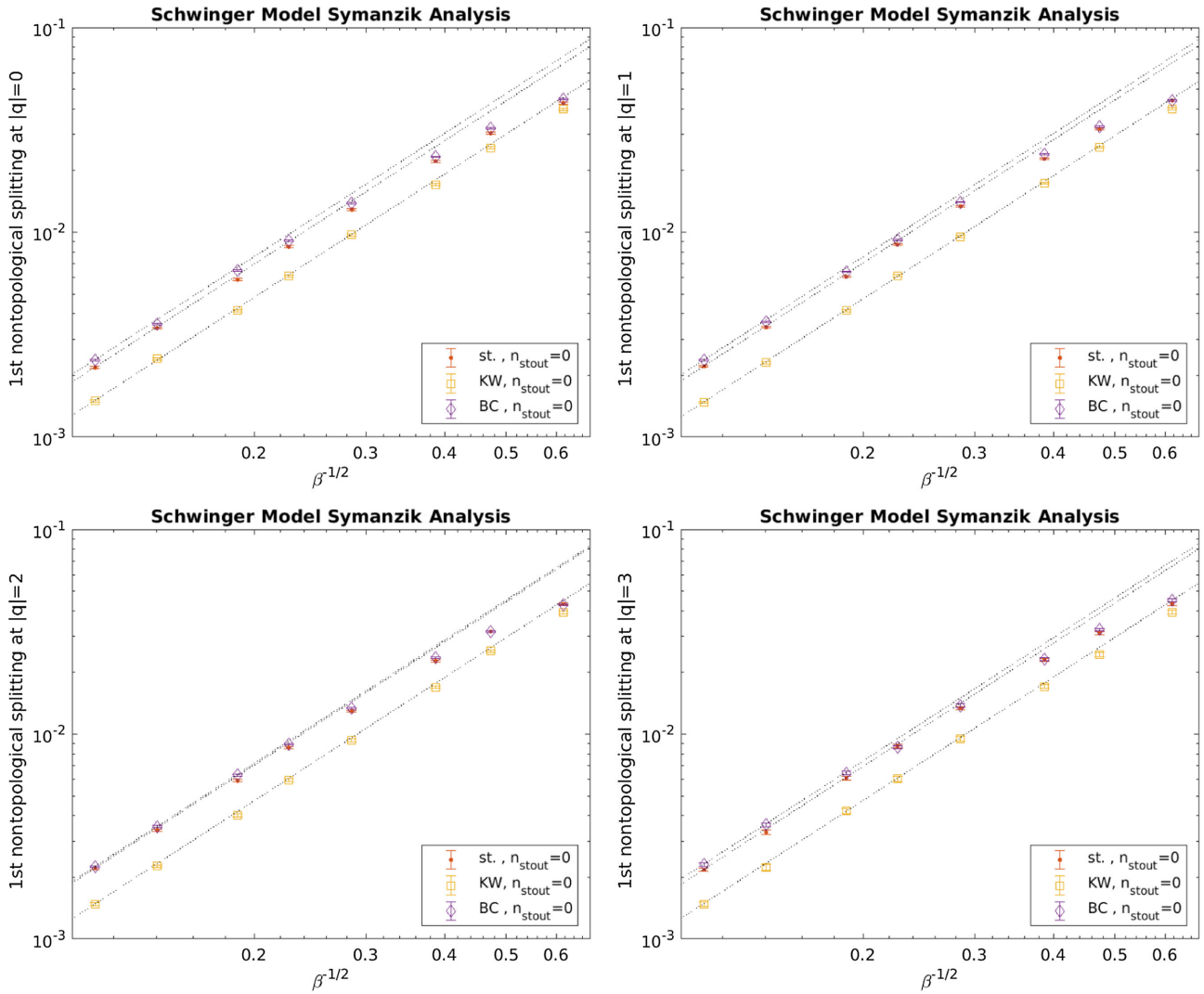

FIG. 14. First nontopological splitting $a\delta_{|q|+1}$ at $|q| = 0$, 1, 2, 3 versus a for $n_{\text{stout}} = 0$. Each dotted line represents a power law $a\delta \propto a^2$, adjusted to go through the leftmost data point.

VII. CONCLUSIONS AND OUTLOOK

The goal of this paper has been to assess how a continuum Dirac operator eigenvalue is split into a pair of near-degenerate eigenvalues for staggered, Karsten-Wilczek and Boriçi-Creutz fermions in 2D. On typical gauge backgrounds staggered taste splittings were found to diminish exponentially in the gradient flow time τ, provided the latter is not too large (see Fig. 3 and Ref. [45]). At a given level of smearing (or gradient flow time in lattice units; we chose $\tau/a^2 = 0, 0.25, 0.75$) the taste breaking effects were found to disappear in the continuum limit, albeit not necessarily as fast as standard arguments would suggest.

We find that it makes a difference whether the underlying continuum mode is a would-be zero mode ("wbz") or a nontopological ("ntm") mode. For wbz modes the splitting disappears as $\delta_{\text{wbz}} \propto a$ for all three actions without link smearing, and $\delta_{\text{wbz}} \propto a^2$ for all three actions with smearing. This observation is disturbing, as it challenges the standard view [7–11] that a fixed level of smearing does not change the Symanzik universality class of a given fermion operator.

For nontopological modes we end up with the unexpected observation that only the staggered action with link smearing scales asymptotically as $\delta_{\text{ntm}} \propto a^2$, while our data for unsmeared staggered fermions and for KW and BC with and without link smearing suggest $\delta_{\text{ntm}} \propto a$. The conjectured powers in the asymptotic Symanzik law $\delta \propto a^p$ are summarized in Table III, and we recall that subleading corrections were seen in all cases, in particular with smearing.

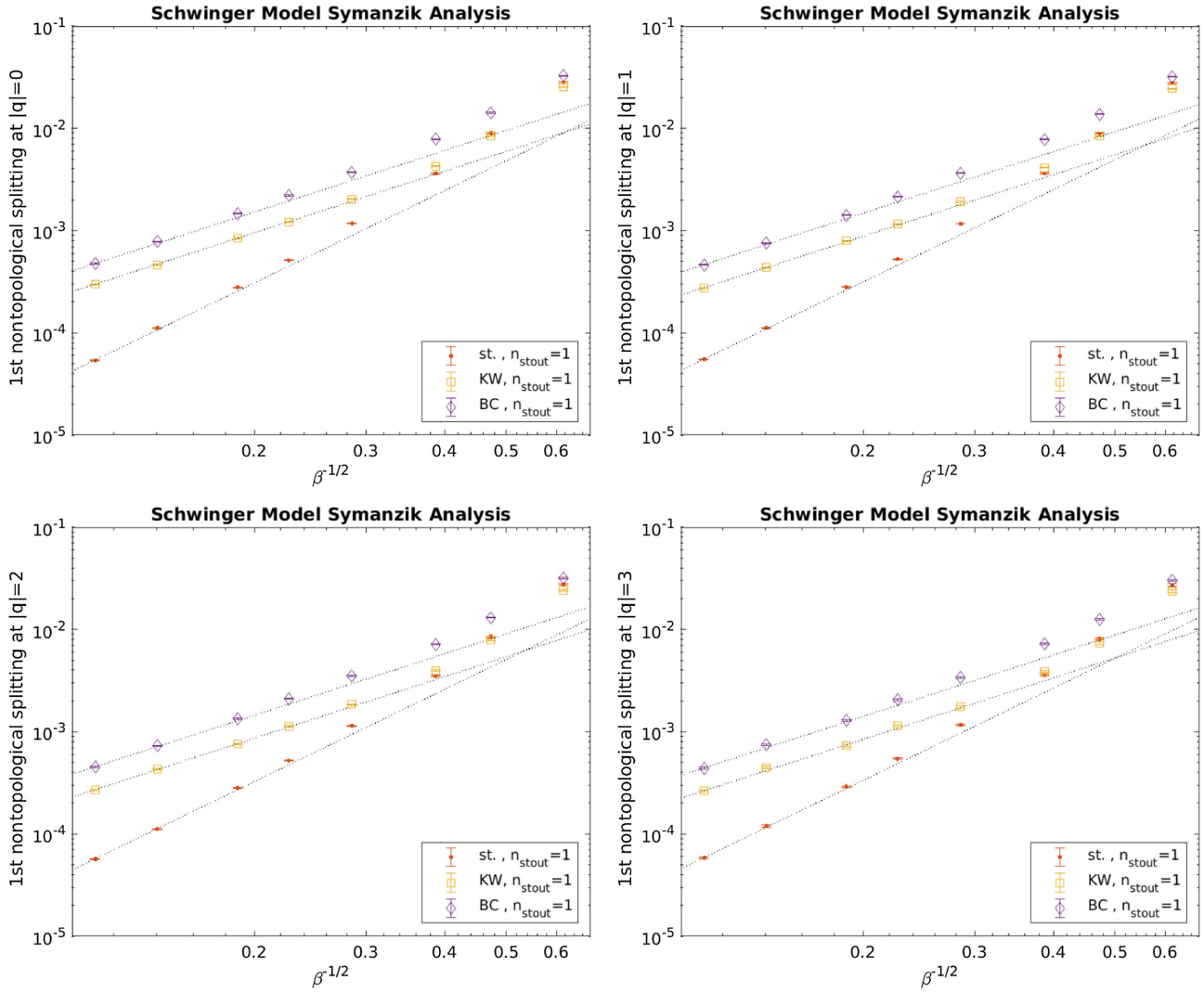

FIG. 15. Same as Fig. 14 but for $n_{\mathrm{stout}} = 1$. For D_{st} the dotted line is a power law $a\delta \propto a^3$, for D_{KW} and D_{BC} it is $a\delta \propto a^2$, always adjusted to the leftmost data point.

We emphasize that our results for KW and BC fermions are for the bare actions, i.e. without marginal counterterms (see e.g. Ref. [50] for details). Including such counterterms might change some of the entries in the lower two lines of Table III. Unfortunately, the coefficients of these counterterms are not known in 2D (neither perturbatively nor nonperturbatively, neither with nor without stouting). For staggered fermions there are no such counterterms, and the conjectured change from $p = 1$ to $p = 2$ with smearing remains mysterious.

Evidently, our findings are unexpected and deserve due diligence. It is conceivable that our data do not reflect the true asymptotic behavior. This, however, would be surprising, since our lattices are rather fine compared to previous investigations (we bridge a factor $\beta_{\mathrm{max}}/\beta_{\mathrm{min}} = 25$, tantamount to a factor 5 between the largest/smallest lattice spacing). Assuming there is no technical issue with our code[11] it seems that the interplay between smearing and subleading corrections to asymptotic Symanzik scaling deserves a closer look (based on precise data). For a discussion of logarithmic corrections in QCD-like theories see Refs. [51–56].

[11]Of course, we started scrutinizing our code. We mentioned in Sec. II that we checked our simulation data against analytic results of Ref. [40]. We carefully checked the implementation of the fermion operators against those used in Ref. [28]. Also the smearing seems fine; when applied to a purely gluonic observable it seems to imply beautiful Symanzik scaling at each smearing level (including $n_{\mathrm{stout}} = 0$), see the Appendix for details. Last but not least, the eigenvalue determination could be flawed. But we use canned routines, and we checked that the functions `eig` and `eigs` in MATLAB (which use different algorithms) yield identical results.

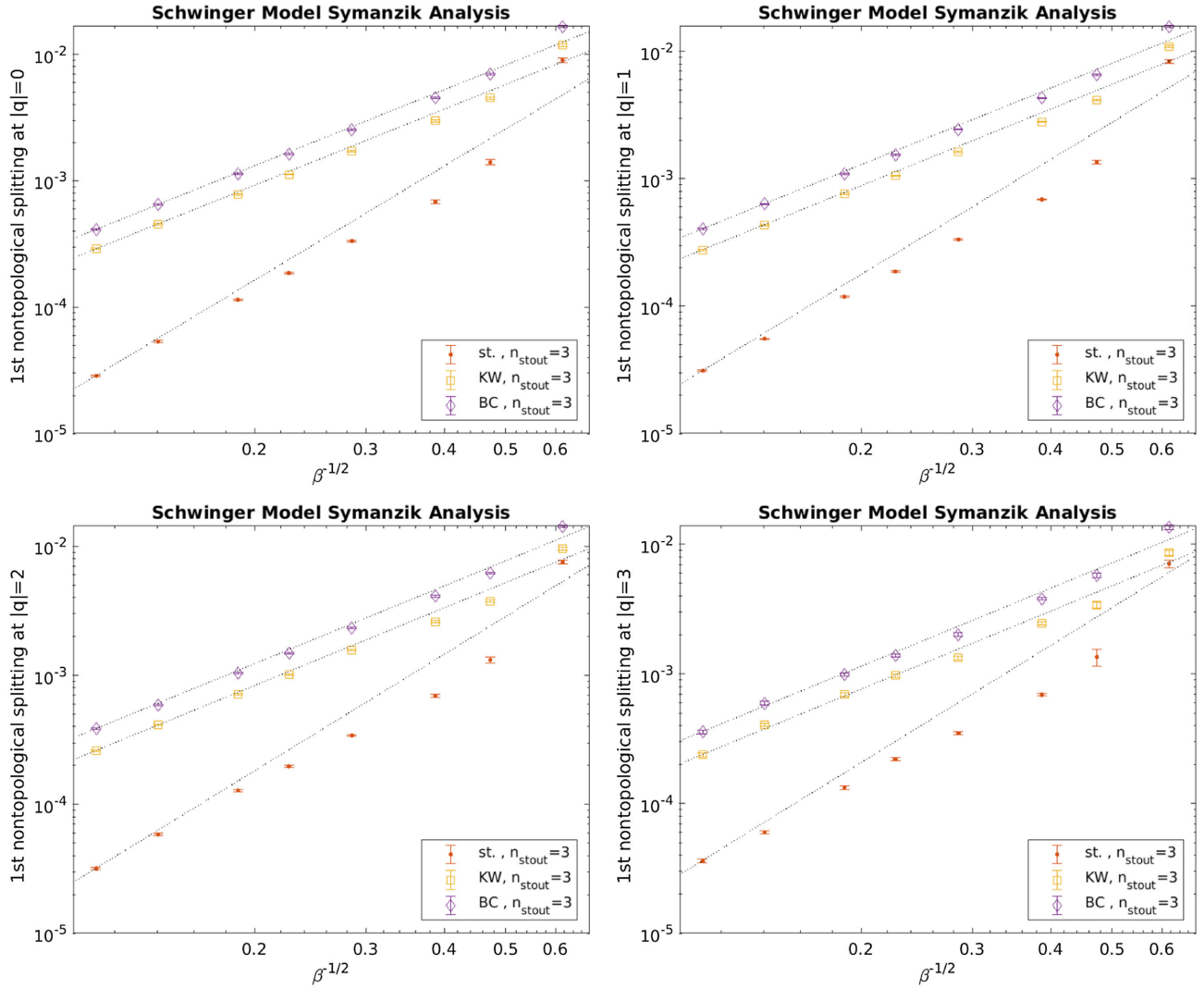

FIG. 16. Same as Fig. 14 but for $n_{\mathrm{stout}} = 3$. For D_{st} the dotted line is a power law $a\delta \propto a^3$, for D_{KW} and D_{BC} it is $a\delta \propto a^2$, always adjusted to the leftmost data point.

Several research strategies may shed some light on the conundrum presented in this paper. First, it would be interesting to know whether the $|q|$ real-valued eigenvalues in the physical branch of an unimproved Wilson fermion (which belong to "would-be zero modes") vanish in the continuum limit like $\lambda_{\mathrm{wbz}} \propto a$, and whether tree-level or one-loop improvement would change this behavior to $\lambda_{\mathrm{wbz}} \propto a\log(a)$ or $\lambda_{\mathrm{wbz}} \propto a\log^2(a)$, as the Symanzik surmise suggests. Again, one would not expect to find any dependence on the amount of smearing (keeping the flow time fixed in lattice units, $\tau/a^2 = \mathrm{const}$), but surprises may happen. Second, it would be interesting to repeat the analysis of this paper with a spectroscopy based measure of the taste splitting (defined as the difference between the squared pion masses with different taste structure), for all three fermion formulations, and to check whether the results depend on the amount of link smearing. With smearing one should be prepared to see large corrections, to the point that it becomes a challenge to determine the asymptotic Symanzik power p.

TABLE III. Power p in the asymptotic Symanzik scaling law $\delta \propto a^p$, as suggested by our data for staggered, KW and BC fermions. The behavior without and with link smearing, and for would-be zero modes versus nontopological modes is listed separately.

	$n_{\mathrm{stout}} = 0$		$n_{\mathrm{stout}} = 1, 3$	
	wbz	ntm	wbz	ntm
$\delta_{\mathrm{stag}} \propto a^p$	1	1	2	2
$\delta_{\mathrm{KW}} \propto a^p$	1	1	2	1
$\delta_{\mathrm{BC}} \propto a^p$	1	1	2	1

ACKNOWLEDGMENTS

One of us (S. D.) happily acknowledges a useful conversation with Steve Sharpe on the research reported in this article.

DATA AVAILABILITY

No data were created or analyzed in this study.

APPENDIX: SYMANZIK SCALING OF TOPOLOGICAL CHARGE Z-FACTOR

A lattice regularized topological charge density $q(x)$ or (global) charge q renormalizes multiplicatively relative to its continuum counterpart [57,58]. The respective Z-factor can be read off from the histogram of q_{raw} as defined in (3). This is exemplified in Fig. 17 for $(\beta, n) = (5.0, 0)$. For instance, if the peaks are near $\pm 0.9, \pm 1.8, \pm 2.7, \ldots$, then the choice $Z = 1/0.9 \simeq 1.11$ would make Zq_{raw} peak near integer-valued numbers. To formalize this observation, one defines

$$\chi^2(Z) = \sum_U \left(\mathrm{round}(Zq^{(n)}_{\mathrm{raw}}[U]) - Zq^{(n)}_{\mathrm{raw}}[U] \right)^2 \qquad \text{(A1)}$$

where the sum is over all configurations in a given ensemble. The local minimum of χ^2 at $Z > 1$ defines Z, and this renormalization condition was also used in Refs. [59–62]. For $(\beta, n) = (5.0, 0)$ Fig. 18 indicates that

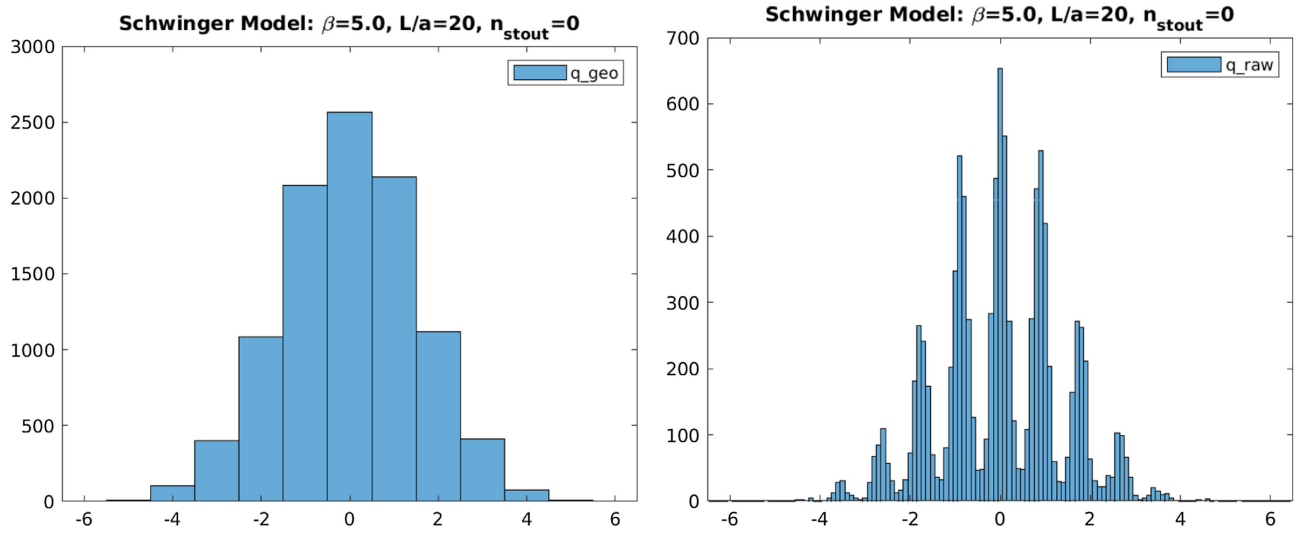

FIG. 17. Histogram of the integer-valued topological charge q_{geo} (left) and of the real-valued charge q_{raw} (right) in the ensemble $\beta = 5.0$, $L/a = 20$, $n_{\mathrm{stout}} = 0$ with 10 000 configurations.

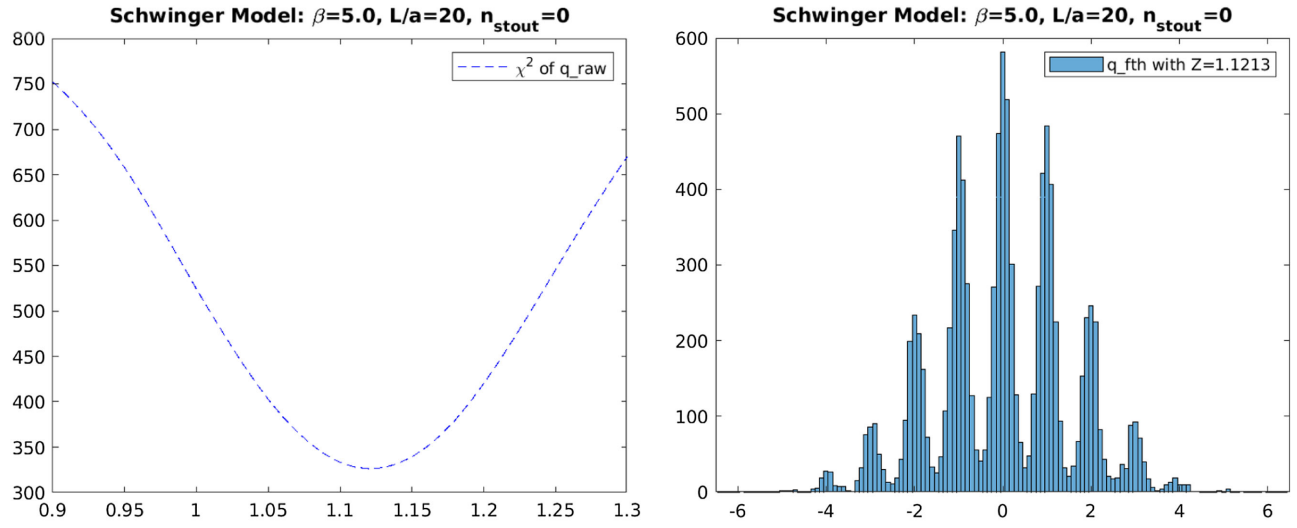

FIG. 18. Dependence of χ^2 on Z for $n_{\mathrm{stout}} = 0$; the abscissa of its minimum defines Z (left). The resulting histogram of Zq_{raw} (right), before rounding, for the same ensemble as in Fig. 17.

TABLE IV. Results for $Z^{(n)}$ in the cutoff effect study as defined in Table I. Every column comprises three ensembles of 10 000 configurations each, subject to either 0, 1 or 3 stout steps.

β	3.2	5.0	7.2	12.8	20.0	28.8	51.2	80.0
L/a	16	20	24	32	40	48	64	80
$Z^{(n=0)}$	1.2032(50)	1.1213(13)	1.0776(7)	1.0412(4)	1.0262(2)	1.0177(2)	1.0099(1)	1.0064(1)
$Z^{(n=1)}$	1.0587(15)	1.0273(04)	1.0170(1)	1.0094(0)	1.0061(0)	1.0042(0)	1.0024(0)	1.0016(0)
$Z^{(n=3)}$	1.0183(11)	1.0089(02)	1.0060(1)	1.0035(0)	1.0023(0)	1.0016(0)	1.0009(0)	1.0006(0)

TABLE V. Results for $Z^{(1)}$ in the finite volume study as defined in Table II. Each measurement uses 10 000 configurations and a single stout smearing step.

β	7.2	7.2	7.2	7.2	7.2
L/a	16	20	24	32	40
$Z^{(n=1)}$	1.0171(2)	1.0170(1)	1.0170(1)	1.0171(1)	1.0172(1)

$Z \simeq 1.12$ indeed aligns the peaks in the histogram to integer values.

In Tables IV and V we summarize our results for the topological charge renormalization factor Z for all of our ensembles. The results depend on β and the smearing level n; increasing either one drives the value closer to 1. After Symanzik [46–49] one expects that

$$Z(\beta, n) = 1 + \text{const}_n a^2 + O(a^4) \tag{A2}$$

since both the gauge action (1) and the operator (3) admit leading cutoff effects $\propto a^2$. Our choice of setting the lattice spacing a through the gauge coupling e implies that one may replace a^2 by $1/\beta$ in the Schwinger model. The results tabulated suggest that Z is indeed independent of the volume, whereupon the hypothesis (A2) contains all relevant dependencies.

In Fig. 19 the quantity $Z-1$ is plotted as a function of $\beta^{-1/2}$ in log-log representation. The data support the Symanzik scaling hypothesis (A2), with a prefactor which depends on n. The dotted lines are no fits; they implement the Symanzik power a^2, with a prefactor adjusted to make them (exactly) pass through the leftmost (most continuum-like) data point. The left panel shows that it takes large β-values to see good agreement with Symanzik scaling. Reference [63] proposes to use $\beta_{\text{eff}} = \langle U_\square \rangle \beta$ to set the lattice spacing in the Schwinger model (this shifts all data points a bit to the right). The right panel shows that this improves things slightly for $n_{\text{stout}} = 0$, but the asymptotic behavior (to the far left) is unchanged.

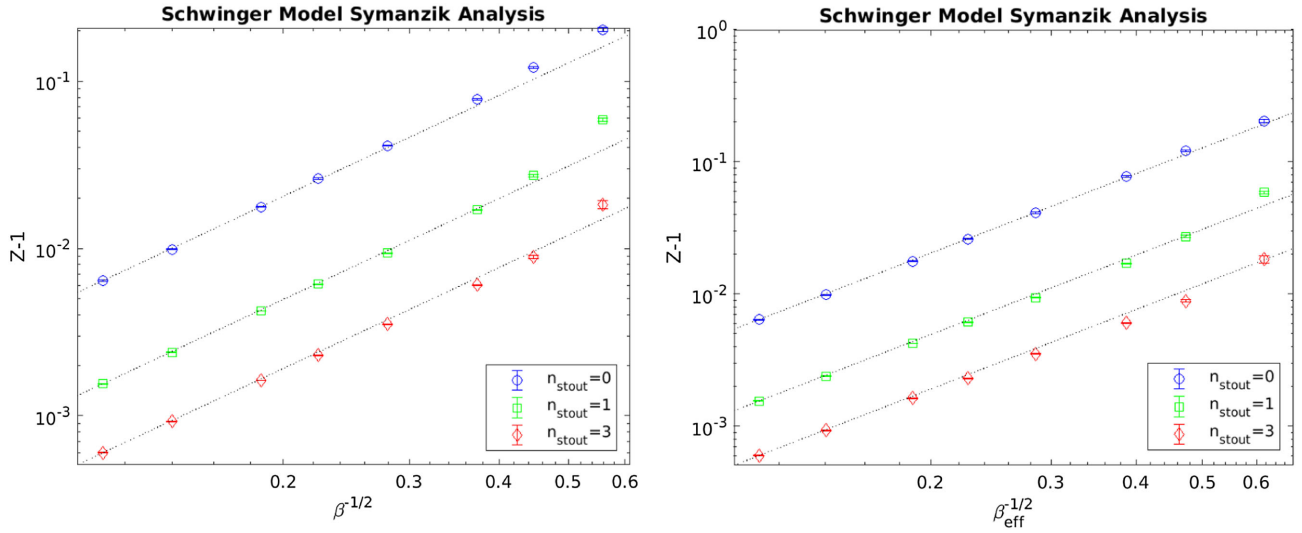

FIG. 19. $Z^{(n)} - 1$ versus two varieties of a (left $\beta^{-1/2}$, right $\beta_{\text{eff}}^{-1/2}$, see text), for $n_{\text{stout}} = 0, 1, 3$. The dotted lines are power laws $\propto a^2$ passing through the leftmost data point.

Overall, both panels illustrate the applicability of the Symanzik scaling hypothesis (A2) for the quantity $Z-1$ at each smearing level $n_{\mathrm{stout}} \in \{0, 1, 3\}$. The reluctance to assume Symanzik scaling and the dependence of the power p on n_{stout} that were reported in the main investigation are thus genuine to the fermion operators and unrelated to the smearing procedure.

[1] L. Susskind, Phys. Rev. D **16**, 3031 (1977).
[2] L. H. Karsten and J. Smit, Nucl. Phys. **B183**, 103 (1981).
[3] H. S. Sharatchandra, H. J. Thun, and P. Weisz, Nucl. Phys. **B192**, 205 (1981).
[4] H. Kluberg-Stern, A. Morel, O. Napoly, and B. Petersson, Nucl. Phys. **B220**, 447 (1983).
[5] M. F. L. Golterman and J. Smit, Nucl. Phys. **B245**, 61 (1984).
[6] J. Smit and J. C. Vink, Nucl. Phys. **B286**, 485 (1987).
[7] T. Blum, C. E. Detar, S. A. Gottlieb, K. Rummukainen, U. M. Heller, J. E. Hetrick, D. Toussaint, R. L. Sugar, and M. Wingate, Phys. Rev. D **55**, R1133 (1997).
[8] K. Orginos and D. Toussaint, Phys. Rev. D **59**, 014501 (1999).
[9] J. F. Lagae and D. K. Sinclair, Phys. Rev. D **59**, 014511 (1999).
[10] G. P. Lepage, Phys. Rev. D **59**, 074502 (1999).
[11] F. Knechtli and A. Hasenfratz, Phys. Rev. D **63**, 114502 (2001).
[12] N. Kawamoto and J. Smit, Nucl. Phys. **B192**, 100 (1981).
[13] W. J. Lee and S. R. Sharpe, Phys. Rev. D **60**, 114503 (1999).
[14] L. H. Karsten, Phys. Lett. **104B**, 315 (1981).
[15] F. Wilczek, Phys. Rev. Lett. **59**, 2397 (1987).
[16] M. Creutz, J. High Energy Phys. 04 (2008) 017.
[17] A. Borici, Phys. Rev. D **78**, 074504 (2008).
[18] H. B. Nielsen and M. Ninomiya, Nucl. Phys. **B185**, 20 (1981); **B195**, 541(E) (1982).
[19] H. B. Nielsen and M. Ninomiya, Nucl. Phys. **B193**, 173 (1981).
[20] G. P. Lepage, arXiv:1111.2955.
[21] K. Cichy, J. Gonzalez Lopez, K. Jansen, A. Kujawa, and A. Shindler, Nucl. Phys. **B800**, 94 (2008).
[22] J. H. Weber, Properties of minimally doubled fermions, Ph.D. thesis, arXiv:1706.07104.
[23] J. H. Weber, Proc. Sci., LATTICE2016 (**2017**) 250.
[24] M. Pernici, Phys. Lett. B **346**, 99 (1995).
[25] B. C. Tiburzi, Phys. Rev. D **82**, 034511 (2010).
[26] M. Creutz, T. Kimura, and T. Misumi, J. High Energy Phys. 12 (2010) 041.
[27] S. Dürr and J. H. Weber, Phys. Rev. D **102**, 014516 (2020).
[28] S. Dürr and J. H. Weber, Phys. Rev. D **105**, 114511 (2022).
[29] J. Smit and J. C. Vink, Phys. Lett. B **194**, 433 (1987).
[30] J. Smit and J. C. Vink, Nucl. Phys. **B303**, 36 (1988).
[31] M. L. Laursen, J. Smit, and J. C. Vink, Nucl. Phys. **B343**, 522 (1990).
[32] S. J. Hands and M. Teper, Nucl. Phys. **B347**, 819 (1990).
[33] J. S. Schwinger, Phys. Rev. **128**, 2425 (1962).
[34] J. H. Lowenstein and J. A. Swieca, Ann. Phys. (N.Y.) **68**, 172 (1971).
[35] M. M. Ansourian, Phys. Lett. **70B**, 301 (1977).
[36] H. Dilger, Phys. Lett. B **294**, 263 (1992).
[37] H. Dilger, Int. J. Mod. Phys. C **06**, 123 (1995).
[38] S. Dürr, Phys. Rev. D **85**, 114503 (2012).
[39] T. Eichhorn and C. Hoelbling, Proc. Sci., LATTICE2021 (**2022**) 573.
[40] S. Elser, The local bosonic algorithm applied to the massive Schwinger model, Ph.D. thesis, arXiv:hep-lat/0103035.
[41] C. Morningstar and M. J. Peardon, Phys. Rev. D **69**, 054501 (2004).
[42] E. Follana, A. Hart, and C. T. H. Davies, Phys. Rev. Lett. **93**, 241601 (2004).
[43] S. Dürr, C. Hoelbling, and U. Wenger, Phys. Rev. D **70**, 094502 (2004).
[44] M. Lüscher, J. High Energy Phys. 08 (2010) 071; 03 (2014) 092(E).
[45] M. Ammer and S. Dürr, Proc. Sci. LATTICE2022 (**2023**) 291.
[46] K. Symanzik, Nucl. Phys. **B226**, 187 (1983).
[47] K. Symanzik, Nucl. Phys. **B226**, 205 (1983).
[48] G. Curci, P. Menotti, and G. Paffuti, Phys. Lett. **130B**, 205 (1983); **135B**, 516(E) (1984).
[49] M. Lüscher and P. Weisz, Commun. Math. Phys. **97**, 59 (1985); **98**, 433(E) (1985).
[50] J. H. Weber, Proc. Sci., LATTICE2023 (**2024**) 353.
[51] J. Balog, F. Niedermayer, and P. Weisz, Phys. Lett. B **676**, 188 (2009).
[52] J. Balog, F. Niedermayer, and P. Weisz, Nucl. Phys. **B824**, 563 (2010).
[53] J. Balog, F. Niedermayer, M. Pepe, P. Weisz, and U. J. Wiese, J. High Energy Phys. 11 (2012) 140.
[54] N. Husung, P. Marquard, and R. Sommer, Eur. Phys. J. C **80**, 200 (2020).
[55] N. Husung, P. Marquard, and R. Sommer, Phys. Lett. B **829**, 137069 (2022).
[56] N. Husung, Eur. Phys. J. C **83**, 142 (2023); **83**, 276(E) (2023).
[57] M. Campostrini, A. Di Giacomo, and H. Panagopoulos, Phys. Lett. B **212**, 206 (1988).
[58] M. Campostrini, A. Di Giacomo, H. Panagopoulos, and E. Vicari, Nucl. Phys. **B329**, 683 (1990).
[59] A. Di Giacomo and E. Vicari, Phys. Lett. B **275**, 429 (1992).
[60] B. Alles, M. Campostrini, A. Di Giacomo, Y. Gunduc, and E. Vicari, Phys. Rev. D **48**, 2284 (1993).
[61] L. Del Debbio, H. Panagopoulos, and E. Vicari, J. High Energy Phys. 08 (2002) 044.
[62] S. Dürr, Z. Fodor, C. Hoelbling, and T. Kurth, J. High Energy Phys. 04 (2007) 055.
[63] P. de Forcrand, J. E. Hetrick, T. Takaishi, and A. J. van der Sijs, Nucl. Phys. B, Proc. Suppl. **63**, 679 (1998).